Astronomy & Astrophysics manuscript no. 30717˙corrv2
June 7, 2018

86 GHz SiO maser survey of late-type stars in the Inner Galaxy. IV. SiO emission and infrared data for sources in the Scutum and Sagittarius-Carina arms, $20° < l < 50°$ ⋆

Messineo, M.[1,2] ⋆⋆, H. J., Habing[2], L. O., Sjouwerman[3], A., Omont,[4], and K. M., Menten[5]

[1] Key Laboratory for Researches in Galaxies and Cosmology, University of Science and Technology of China, Chinese Academy of Sciences, Hefei, Anhui, 230026, China e-mail: messineo@ustc.edu.cn
[2] Leiden Observatory, PO Box 9513, 2300 RA Leiden, The Netherlands
[3] National Radio Astronomy Observatory, PO Box 0, Socorro NM 87801, USA
[4] Institut d'Astrophysique de Paris, CNRS, 98bis boulevard Arago, 75014 Paris, France
[5] Max-Planck-Institut für Radioastronomie, Auf dem Hügel 69, D-53121 Bonn, Germany

Received 2011/ Accepted

ABSTRACT

We present an 86 GHz SiO ($v = 1, J = 2 \rightarrow 1$) maser search toward late-type stars located within $|b| < 0.^{\circ}5$ and $20° < l < 50°$. This search is an extension at longer longitudes of a previously published work. We selected 135 stars from the MSX catalog using color and flux criteria and detected 92 (86 new detections). The detection rate is 68%, the same as in our previous study.
The last few decades have seen the publication of several catalogs of point sources detected in infrared surveys (MSX, 2MASS, DENIS, ISOGAL, WISE, GLIMPSE, AKARI, and MIPSGAL). We searched each catalog for data on the 444 targets of our earlier survey and for the 135 in the survey reported here. We confirm that, as anticipated, most of our targets have colors typical of oxygen-rich asymptotic giant branch (AGB) stars. Only one target star may have already left the AGB. Ten stars have colors typical of carbon-rich stars, meaning a contamination of our sample with carbon stars $\lesssim 1.7$ %.

Key words. stars: AGB and post-AGB, stars: late-type, stars: circumstellar matter, catalogs, masers, Galaxy: kinematics and dynamics

1. Introduction

Asymptotic giant branch (AGB) stars are rare, but they are among the brightest stars at infrared wavelengths. They lose mass at rates from 10^{-9} $M_{\odot}$ yr^{-1} up to 10^{-4} $M_{\odot}$ yr^{-1}, and are often surrounded by circumstellar envelopes where maser emission from SiO, H_2O, and OH may arise. Maser observations provide information on the angular distribution and accurate line-of-sight velocities of AGB stars. A number of maser surveys have been carried out to measure stellar line-of-sight velocities toward the inner Galaxy (e.g., Lindqvist et al. 1992; Blommaert et al. 1994; Sevenster et al. 2001, 1997a,b; Sjouwerman et al. 1998; Izumiura et al. 1999; Deguchi et al. 2000b,a). These surveys were mostly aimed at the detection of OH/IR stars [1]. About 800 OH/IR stars were detected with the first largescale blind surveys at 1612 MHz by Sevenster et al. (e.g., 1997a,b, 2001). Kinematic modelings of that data allowed for constraints on the Galactic bars properties and yielded quantitative parameters of the bar (e.g., Sevenster 1999; Debattista et al. 2002; Habing et al. 2006).

Stars of the AGB also emit SiO maser emission at 43 and 86 GHz and more stars show this maser than that of OH (Habing et al. 2006). SiO-maser surveys have been carried out around the years 2000-2002 with the Nobeyama telescope (Deguchi et al. 2000c). These surveys mainly targeted IRAS point sources and suffered from significant confusion near the Galactic plane. Large infrared surveys of the Galactic plane with less confusion than IRAS were already available at the beginning of the year 2000, when we embarked on a search for 86 GHz SiO masers directed at targets selected from the ISOGAL (Omont et al. 2003; Schuller et al. 2003) and MSX catalogs (Egan et al. 1999, 2003). We detected 255 SiO maser lines in 444 targets in the area $|b| < 0.^{\circ}5$ and $-4° < l < +30°$ (Messineo et al. 2002). The targets were selected to be complementary to the previous OH/IR surveys, in other words, sources with the reddest mid- and near-infrared colors were excluded.

In 2003, an additional dataset of SiO masers at 86 GHz was obtained to extend the survey to longer longitudes ($20° < l < 50°$). A kinematic analysis of this dataset, together with that of Messineo et al. (2002), is presented in Habing et al. (2006). In this paper we publish the list of these 92 SiO maser detections between $20° < l < 50°$. We also discuss the infrared properties of all our 444 previous targets and the 135 new targets as they are found in the new infrared surveys, MSX, 2MASS, DENIS, ISOGAL, WISE, GLIMPSE, AKARI, and MIPSGAL.

In Sect. 2, we present the target selection and radio observations of the 135 new targets, and in Sect. 3 the identifications of counterparts from available large infrared surveys of the 444 + 135 targets in the Galactic plane. In Sect. 4, we briefly describe the detection rate and properties of the newly detected SiO maser

⋆ The full Table 3 is only available in electronic form at the CDS via anonymous ftp to cdsarc.u-strasbg.fr (130.79.128.5) or via http://cdsweb.u-strasbg.fr/cgi-bin/qcat?J/A+A/xxx/xxx.

⋆⋆ MM is currently employed by the University of Science and Technology of China. This works was partially carried out during her PhD thesis (2000-2004) in Leiden.

[1] AGB stars with OH maser emission in the 1612 MHz line, mostly undetected at visual wavelengths, but bright in the IR.

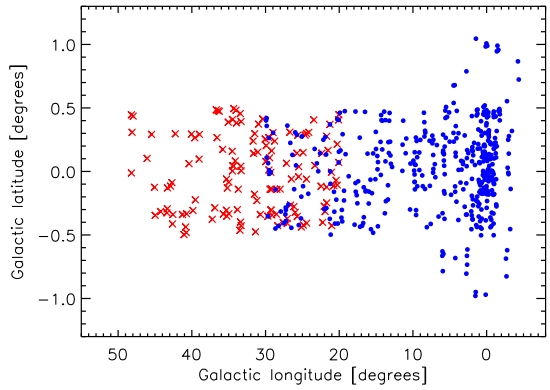

Fig. 1. Galactic coordinates of the new targets (red crosses). For comparison the targets in Messineo et al. (2002) (blue dots) are also shown.

lines, and in Sect. 5 we discuss the infrared colors of all 579 targeted stars. Finally, a summary is provided in Sect. 6.

2. 86 GHz SiO masers in the 2003 IRAM campaign

In our previous paper, we color-selected bright ([15] < 3.4 mag) stars in the ISOGAL [15] versus (K_s−[15]) diagram, and ISOGAL [15] versus ([7] − [15]) diagram, so as to exclude the reddest sources since those usually do not show SiO but OH maser emission; we defined a similar selection with MSX colors and fluxes. Sources for the 2003 SiO observations were selected from Version 1.2 of the Midcourse Space Experiment point source catalog (MSX-PSC, Egan et al. 1999) by following the color criteria of our previous paper. Flux densities in D-band range from 0.56 Jy (3.78 mag) to 2.12 Jy (2.34 mag). A number of 127 targets are observed for the first time; eight targets are reobservations of targets in Messineo et al. (2002). Due to visibility limits from the IRAM 30-m telescope, there is a lower limit to the target longitude of about −4°. We restricted the latitude mostly to the limits −0.°5 and 0.°5. Locations of the targets are shown in Fig. 1. Evidence of variability is available from DENIS/2MASS near-infrared measurements; the majority of our targets are long-period variables (see Messineo et al. 2004).

The observations were carried out with the IRAM 30-m telescope on Pico Veleta in Spain between October and November 2003, under the proposal number 021-03 (30 hours). Telescope settings and observational strategy were the same as described in Messineo et al. (2002). Two receivers were used to observe the two orthogonal linear polarizations. To each receiver, we attached the low-resolution analog filter bank with a resolution of 3.5 km s^{-1} and a coverage of 890 km s^{-1}, and in parallel the autocorrelator with a resolution of 1.1 km s^{-1} and a bandwidth 973 km s^{-1}. The IRAM beam at 86 GHz has a full width at half-maximum (FWHM) of 29″. The observations were made in wobbler switching mode, with the wobbler throw varying between 100″ and 200″. Integration times ranged from 10 to 24 minutes per source; the average spectral noise is 0.012 K with a σ = 0.003 K. The conversion factor from antenna temperatures to flux densities is 6.2 Jy K^{-1}. Typically, the SiO maser line has a width of a few km s^{-1}; therefore, the line is not resolved in the spectra from the filter bank (one or two channels). We considered, as a detection, only lines simultaneously detected in the spectra from the filter bank and in those from the autocorrelator. Data analysis was carried out with the CLASS package within the GILDAS software. Maser parameters, such as velocities, FWHMs, and integrated area below the line emission (A), were estimated by fitting the detected lines with a Gaussian function.

Table 1 lists the 92 detections at 86 GHz (86 new detections), while Table 2 lists the 43 non-detected targets (41 observed for the first time). The spectra of the detected targets are shown in Fig. A.1. Since the lists by Messineo et al. (2002) contain 444 targets, Table 1 begins with the identifier number 445.

3. Infrared counterparts to the targets searched for SiO masers

We searched for available mid-infrared data for the 127 new targets as well as for the 444 targets of Messineo et al. (2002). We used the final MSX release (version 2.3, catalog V/114 in CDS, Egan et al. 2003), the ISOGAL catalog (Schuller et al. 2003; Omont et al. 2003), the GLIMPSE catalog (catalog II/293 in CDS, Churchwell et al. 2009; Benjamin et al. 2003), the AllWISE Data Release (catalog II/328 in CDS, Wright et al. 2010; Cutri & et al. 2013), the AKARI/IRC All-Sky Survey point source catalog v.1.0 (Ishihara et al. 2010), and the MIPSGAL 24 μm catalog by Gutermuth & Heyer (2015).

The targets had been selected from MSX catalog Version 1.2, which has an astrometric accuracy of ∼ 2″ (resolution of 18.″3, Egan et al. 1999). For comparison, the targets selected from the ISOGAL catalog of Messineo et al. (2002) had a subarcsec accuracy (resolution of 1″, Messineo et al. 2004). Since 2MASS sources have been astrometrically cross-correlated with WISE and GLIMPSE targets, we can now check the earlier 2MASS matches to the MSX sources (see Appendix B). The MSX camera had a spatial resolution of 18.″3, while the beam of the IRAM 30-m telescope had a FWHM of 29″. MSX counterparts were found within 14.″5 for 566 of the 571 targets. Excluding the upper limits we have 280 targets with good measurements in all four MSX bands. MSX magnitudes are obtained adopting the following zero-points: 58.49 Jy in the A band (8.26μm), 26.51 Jy in C-band (12.12 μm), 18.29 Jy in D band, (14.65 μm), and 8.80 Jy in E band (21.41 μm) (Egan et al. 1999). WISE has a resolution of 6″, and a final astrometric accuracy better than 0.″5. It imaged the sky at 3.4 μm ($W1$-band), 4.6 μm ($W2$-band), 12 μm ($W3$-band), and 22 μm ($W4$-band) with a sensitivity of 0.08, 0.11, 1, and 6 mJy, and typical saturation thresholds at 0.18, 0.36, 0.88, and 12 Jy. 93% of our targets have unique WISE matches within 10.″0. A few MSX data points were resolved by WISE into several components; two WISE matches were available for 5% of the targets. The closest match was retained, which is also, in all but two cases, the brightest match in the $W3$ band (see Appendix B). For the Galactic Infrared Midplane Survey Extraordinaire (GLIMPSE), the Infrared Array Camera (IRAC) on board of the Spitzer Space Observatory was used to image the plane of the Galaxy at 3.6, 4.5, 5.8, and 8.0 μm with a spatial resolution of 1.″2, and a sensitivity of 0.2, 0.2, 0.6, and 0.4 mJy and saturation thresholds of 180, 190, 570, and 470 mJy. MSX measurements in the 8 μm (band-A) range from 6.35 to 2.08 mag, with a Gaussian peak at 3.55 mag and a σ = 0.80 mag. We considered only GLIMPSE stars with [8.0] < 6.0 mag as safe identifications. A second iteration with a fainter threshold was not needed. GLIMPSE counterparts were found for 76% of the targets using a search radius of 10″ and selecting the closest. For 63% of the targets, the MSX, WISE, and GLIMPSE selected counterparts are unique within the search radius. For targets selected from the MSX catalog, with the 2MASS magnitudes and positions, we searched for additional

Table 1. Sources with detected 86 GHz SiO maser emission.

ID	MSXID	V_{LSR} [km s^{-1}]	T_a [K]	rms [K]	A [K km s^{-1}]	FWHM [km s^{-1}]	Obs.Date [ddmmyy]	SIMBAD alias
445	*G*020.0327+00.4456	129.7	0.058	0.011	0.29±0.03	4.8±0.6	031003	
446	*G*020.2682+00.2141	102.5	0.053	0.014	0.33±0.05	6.2±1.0	031003	
447	*G*020.2609-00.1068	123.2	0.080	0.009	0.45±0.04	5.4±0.5	031003	
448	*G*021.0506-00.0063	28.7	0.293	0.010	1.22±0.03	4.4±0.1	031003	
449[a]	*G*021.6986+00.2768	72.1	0.139	0.014	1.11±0.06	8.2±0.5	101003	2MASSJ18294455−0951203
450	*G*021.5015+00.1654	53.7	0.047	0.010	0.14±0.03	2.6±0.6	031003	
451	*G*021.0134-00.4268	155.8	0.045	0.010	0.18±0.03	3.8±0.7	031003	
452	*G*021.7102-00.1233	96.0	0.062	0.011	0.84±0.06	13.3±1.1	101003	
453	*G*021.6933-00.2472	135.1	0.063	0.013	0.27±0.04	4.1±0.7	101003	
454	*G*021.9071-00.3158	110.2	0.173	0.010	0.57±0.03	3.1±0.2	101003	
455	*G*023.4435+00.4059	112.3	0.069	0.010	0.25±0.04	3.6±0.7	111003/221003	
456	*G*022.4636-00.1162	111.2	0.047	0.009	0.16±0.03	3.5±0.8	101003	
457	*G*022.2467-00.4010	22.2	0.045	0.010	0.30±0.05	9.1±1.6	101003	
458	*G*023.3004+00.0466	128.6	0.094	0.008	0.50±0.04	6.4±0.7	101003	
459	*G*024.1345+00.3074	141.7	0.113	0.020	0.92±0.11	10.4±1.4	111003	
460	*G*024.4277+00.2976	52.6	0.083	0.009	0.77±0.05	13.2±0.9	101003	
461	*G*024.4455-00.0612	53.7	0.104	0.014	0.47±0.05	4.1±0.6	121003	
462[b]	*G*025.6246+00.2846	33.0	0.081	0.011	0.57±0.05	7.8±0.9	121003	IRAS 18343−0624
463	*G*025.4894+00.0372	-30.0	0.047	0.010	0.21±0.03	4.0±0.5	121003/031103	
464	*G*025.7324+00.1434	-0.7	0.064	0.008	0.18±0.03	2.7±0.5	111003	
465	*G*025.5134-00.0413	55.8	0.129	0.012	0.45±0.04	3.6±0.4	121003	
466	*G*024.8618-00.4230	1.5	0.034	0.009	0.18±0.03	5.9±1.2	121003	
467	*G*026.6929+00.3095	17.8	0.055	0.012	0.15±0.03	2.4±0.8	121003	
468	*G*025.6894-00.3543	-82.1	0.071	0.008	0.28±0.03	3.9±0.5	101003	
469	*G*025.9663-00.3220	116.7	0.038	0.009	0.40±0.07	12.7±2.2	121003	
470	*G*026.4890-00.0598	75.4	0.086	0.012	0.67±0.06	8.0±0.9	121003	
471	*G*026.1404-00.2768	72.1	0.074	0.012	0.20±0.03	2.4±0.5	121003	
472[c]	*G*027.1520+00.0642	-39.8	0.145	0.012	0.90±0.04	5.6±0.3	221003	LGB99-37
473	*G*026.5920-00.2645	97.1	0.106	0.011	0.57±0.05	6.0±0.7	121003	
474	*G*027.0475-00.4083	67.8	0.060	0.011	0.50±0.07	11.8±2.2	211003/231003	
475	*G*028.0060-00.1391	76.5	0.056	0.012	0.30±0.05	6.0±1.1	221003/031103	
476	*G*027.5895-00.4022	76.5	0.085	0.013	0.52±0.06	7.3±1.2	221003	
477	*G*029.1788+00.1627	40.6	0.111	0.013	0.37±0.04	3.5±0.5	221003	
478	*G*028.3534-00.4268	99.3	0.152	0.031	0.70±0.12	4.7±1.1	211003	
479	*G*029.4346+00.1071	60.2	0.068	0.012	0.38±0.05	6.2±1.0	231003	
480	*G*030.0440+00.2546	113.4	0.187	0.013	0.42±0.03	2.1±0.1	231003	
481[d]	*G*029.1249-00.3432	9.1	0.042	0.010	0.40±0.06	11.7±2.0	221003/031103	F3S05
482	*G*029.9674+00.0786	-46.3	0.309	0.013	1.48±0.05	5.7±0.3	231003	
483[e]	*G*029.2599-00.3034	66.7	0.269	0.013	1.03±0.05	4.3±0.3	221003	S23
484	*G*030.9389+00.3722	70.0	0.066	0.013	0.46±0.06	7.3±1.1	231003	
485	*G*031.4550+00.2974	67.8	0.068	0.012	0.21±0.03	3.0±0.6	231003	
486	*G*031.6752+00.2396	92.8	0.093	0.012	0.85±0.06	10.6±0.9	301003	
487	*G*030.7034-00.3387	65.6	0.127	0.013	0.70±0.06	5.9±0.6	231003	
488	*G*031.1661-00.2286	31.9	0.100	0.011	0.25±0.03	2.2±0.3	231003	
489	*G*031.4963-00.1798	99.3	0.077	0.012	0.47±0.06	9.8±1.2	231003	

Notes. (*a*) Star #449 corresponds to 2MASSJ18294455-0951203, which is classified as an M9-10I/III long period variable (Halpern & Gotthelf 2007). (*b*) Stars #243, #462, #505, and #511 are known SiO maser emitters (Messineo et al. 2002; Deguchi et al. 2004, 2010). (*c*) Star #472 coincides with [LGB99]37, an M9I/III star (López-Corredoira et al. 1999); (*d*) star #481 (SiO V_{lsr}=9.1 km s^{-1}) corresponds to [NGM2011]F3S05, a giant M7III, detected by Negueruela et al. (V_{lsr}=−37 km s^{-1}, 2011). (*e*) Star #483 is a candidate RSG ([CND2009]S23) in the cluster RSGC3 (Clark et al. 2009).

IJK_s magnitudes from the DENIS catalog (using a search radius of 2″, Epchtein et al. 1994), and IJK_s, 7 μm, and 15 μm magnitudes from the combined DENIS-ISOGAL catalog (Omont et al. 2003; Schuller et al. 2003). The 24 μm Spitzer MIPSGAL survey has a spatial resolution of 6″ and a sensitivity from 1.3 mJy to 2 Jy; we found 518 counterparts within a search radius of 10″. Finally, we searched for AKARI/IRC data at 9 μm and 18 μm (Ishihara et al. 2010), and found matches for 473 targets with a search radius of 3.″5. Mid-infrared associations were verified with GLIMPSE charts and with a visual inspection of the stellar energy distribution (SED). In addition, we inspected UKIDSS images (Lucas et al. 2008), that were available for 536 of the 571 targets. All but eight targets appeared as single saturated stars in *K*-band and well centered on the 2MASS position. The collected available infrared measurements of the targets are provided in Table 3 together with the positions from the 2MASS catalog (Skrutskie et al. 2006).

4. SiO maser results

We searched for SiO maser emission at 86 GHz toward our sample of 135 stars and detected 92 SiO maser lines, of which 91 are new detections at 86 GHz. The resulting detection rate is 68% and that compares very well with that in our earlier survey Messineo et al. (66%, 2002).

4.1. Single epoch detection rate and repeated observations

Star #243 (V_{lsr}=110.2 km s^{-1}) coincides with the entry #243 in Messineo et al. (2002), and stars #462 (V_{lsr}=33.0 km s^{-1}), #505 (V_{lsr}=72.1 km s^{-1}), and #511 (V_{lsr}=6.9 km s^{-1}) were detected at 43 GHz by Deguchi et al. (2004) and Deguchi et al. (2010); for each star, measured velocities agree within 1 km s^{-1}. Interestingly, stars #416, #418, #432, #435, #440, #441, and #444 were unsuccessfully searched for SiO emission by Messineo et al. (2002). Five out of these seven stars not detected

Table 1. Continuation of Table 1.

ID	MSXID	V_{LSR} [km s^{-1}]	T_a [K]	rms [K]	A [K km s^{-1}]	FWHM [km s^{-1}]	Obs.Date [ddmmyy]	SIMBAD alias
490	*G*031.3555-00.4748	66.7	0.033	0.010	0.36±0.05	12.4±1.7	231003/031103	
491	*G*033.4182+00.4558	31.9	0.156	0.014	1.03±0.09	14.6±1.5	301003	
492	*G*033.3057+00.3923	78.6	0.199	0.014	1.04±0.05	5.1±0.3	301003	
493	*G*034.0030+00.4828	78.6	0.125	0.014	0.99±0.08	11.1±1.2	301003	
494	*G*033.3397+00.0420	80.8	0.058	0.010	0.12±0.02	2.0±0.4	301003	
495	*G*033.3037+00.0059	84.1	0.131	0.014	0.51±0.05	3.8±0.5	301003	
496	*G*034.3200+00.4951	90.6	0.365	0.014	1.05±0.04	2.5±0.1	301003	
497	*G*034.4797+00.4087	159.0	0.100	0.013	0.77±0.06	8.2±0.7	301003	
498	*G*034.1053+00.0826	66.7	0.156	0.014	0.72±0.05	4.8±0.4	301003	
499	*G*033.6946-00.1398	11.3	0.086	0.014	0.47±0.05	6.1±0.9	301003	
500	*G*033.2976-00.4282	40.6	0.055	0.012	0.25±0.04	5.4±1.2	301003	
501	*G*034.5112+00.1592	50.4	0.110	0.014	0.42±0.05	3.9±0.6	301003	
502	*G*035.0567+00.3877	47.1	0.155	0.012	1.46±0.06	9.1±0.4	021103	
503	*G*034.4224+00.0444	33.0	0.173	0.013	0.68±0.04	3.8±0.3	301003	
504	*G*033.4608-00.4622	45.0	0.227	0.014	0.67±0.04	2.7±0.2	301003	
505[b]	*G*033.8179-00.3008	72.1	0.108	0.014	0.40±0.04	3.4±0.4	301003	[DNZ2010] Mc13−6
506	*G*034.9723-00.0836	71.0	0.092	0.013	0.33±0.04	3.1±0.4	301003	
507	*G*036.2534+00.4734	64.5	0.080	0.012	0.44±0.05	6.5±0.9	021103	
508	*G*035.2797-00.0600	37.4	0.033	0.009	0.14±0.03	4.2±0.8	021103	
509	*G*036.4216+00.4787	-2.8	0.115	0.011	0.31±0.03	2.3±0.2	021103	
510	*G*034.9710-00.3329	53.7	0.140	0.014	0.80±0.05	6.2±0.4	301003	
511[b]	*G*035.2548-00.3518	7.0	0.078	0.012	0.67±0.06	9.2±1.0	021103	IRAS 18544+0150
512	*G*036.8735-00.2866	34.1	0.122	0.011	0.46±0.03	3.4±0.3	021103	
513	*G*037.2240-00.3764	81.9	0.182	0.011	0.73±0.04	4.0±0.4	021103	
514	*G*039.5957+00.2654	27.6	0.048	0.010	0.31±0.04	6.2±1.2	021103	
515	*G*040.0488+00.2936	76.5	0.070	0.013	0.41±0.07	6.9±1.7	021103	
516	*G*039.5220-00.2231	71.0	0.037	0.009	0.18±0.03	4.4±0.9	021103	
517[f]	*G*039.8380-00.3076	28.7	0.163	0.013	0.54±0.06	3.8±0.6	021103	IRAS19027 + 0555
518	*G*040.7140-00.3327	80.8	0.050	0.008	0.19±0.02	3.6±0.5	021103	
519	*G*042.2422+00.2969	55.8	0.176	0.010	0.90±0.03	4.8±0.2	021103	
520	*G*040.7482-00.4813	67.8	0.046	0.009	0.30±0.04	8.2±1.1	021103	
521	*G*041.2734-00.3388	14.6	0.037	0.009	0.20±0.04	6.1±1.6	021103	
522	*G*041.0632-00.4985	36.3	0.075	0.012	0.25±0.04	2.9±0.6	021103	
523	*G*042.5589-00.3387	51.5	0.189	0.011	0.68±0.04	3.6±0.3	021103	
524	*G*042.6182-00.4128	60.2	0.049	0.009	0.17±0.03	3.5±0.7	021103	
525[f]	*G*043.3182-00.2932	62.4	0.424	0.015	2.23±0.05	5.1±0.1	031103	IRAS19091 + 0900
526	*G*044.2448-00.3153	35.2	0.101	0.015	0.80±0.07	9.7±0.8	031103	
527	*G*045.4641+00.2914	36.3	0.195	0.017	0.85±0.06	4.5±0.5	031103	
528	*G*044.9698-00.3452	33.0	0.095	0.014	0.30±0.05	3.3±0.7	031103	
529	*G*046.0606+00.1034	-11.5	0.090	0.012	0.64±0.05	6.6±0.6	031103	
530	*G*047.9533+00.4354	60.2	0.072	0.016	0.45±0.09	10.4±2.5	031103	
416	*G*020.0732+00.4054	131.9	0.159	0.009	0.48±0.03	2.8±0.2	031003	[MHS2002] 416
418	*G*020.0667+00.0706	79.7	0.074	0.008	0.22±0.02	2.7±0.3	031003	[MHS2002] 418
243[b]	*G*021.2558+00.3704	110.2	0.074	0.008	0.31±0.03	4.0±0.4	101003/221003	[MHS2002] 243
432	*G*028.9721+00.3057	98.2	0.038	0.014	0.61±0.11	19.9±5.2	231003	[MHS2002] 432
435	*G*029.5447+00.2644	45.0	0.082	0.013	0.31±0.04	3.5±0.4	231003	[MHS2002] 435
440	*G*029.2733-00.0067	-19.1	0.171	0.013	0.70±0.04	4.3±0.3	231003	[MHS2002] 440

Notes. (*f*) For stars #517 (IRAS 19027+0555) and #525 (IRAS 19091+0900) there are IRAS low resolution spectra (LRS, Kwok et al. 1997); they are classified as class I (incomplete) and class P (red continuum or presence of PAHs) respectively.

in the first epoch had a detectable flux during the second epoch of 86 GHz observations. This implies that 90% of the targets in Messineo et al. (2002) are probably masing stars. In the second epoch the rms noise was lower by a factor of ≈1.3. Flux densities of SiO maser lines are known to vary in phase with the infrared amplitude of the stellar pulsation (e.g., Alcolea et al. 1999). Since the selected sample is made out of long-period variables (Messineo et al. 2004), this single epoch detection rate provides only a lower limit to the actual number of stars capable of hosting SiO masers.

4.2. FWHM of maser lines and candidate RSGs

The 86 GHz maser emission originates in the envelopes of O-rich (Mira-type) AGB stars, as well as in the envelopes of Red Supergiants (RSGs). Weak SiO maser emission is found in semiregular AGB stars (Alcolea et al. 1990). The central star has an extended shell, generated by the strong pulsations where the SiO maser activity takes place. Figure 2 shows the distribution of the FWHMs in comparison to our previous study. Both distributions are compatible with each other, with the FWHM peaking at 4.9 km s^{-1} with a scatter of σ = 2.7 km s^{-1}, and the mean equivalent width (i.e., fitted area / peak) peaking at 4.7 km s^{-1} with a scatter of σ = 2.0 km s^{-1}. There is also a tail with broader FWHMs (> 7 km s^{-1}).

Cooler RSGs with large amplitudes are also strong SiO emitters, and their SiO maser intensity is comparable to that of long period variables (Alcolea et al. 1990). SiO masers associated with RSGs have larger widths (e.g., Verheyen et al. 2012; Le Bertre & Nyman 1990; Alcolea et al. 1990). Alcolea et al. (1999) performed a six-year period monitoring of SiO maser lines and concluded that SiO maser emission contains several 1-2 km s^{-1} peaks over a range of 10 km s^{-1} in LPV-giants or 20-40 km s^{-1} in supergiants. With this statistical argument it should be possible to identify candidate RSGs. However, in many cases lines were detected at the 2.5-3 σ level and it is likely that most of the broad lines are the results of low signal-to-noise obser-

Table 2. Sources not detected at 86 GHz.

ID	MSXID	rms [K]	Obs.date [ddmmyy]
531	*G*020.4122 − 00.0703	0.010	031003
532	*G*020.7490 − 00.1120	0.008	031003
533	*G*022.3430 + 00.1438	0.010	101003
534*[a]	*G*022.0265 − 00.2741	0.011	101003
535*[b]	*G*024.6265 + 00.2856	0.009	121003
536	*G*024.8993 + 00.1493	0.009	121003
537	*G*024.4084 − 00.4077	0.013	121003
538	*G*025.1373 − 00.4375	0.012	121003
539	*G*027.0540 − 00.3708	0.011	211003/231003
540	*G*028.7480 + 00.2394	0.013	221003
541	*G*028.4568 − 00.1409	0.013	211003/031103
542	*G*028.5241 − 00.3361	0.013	221003
543	*G*029.1718 − 00.1392	0.011	221003
544	*G*029.9008 + 00.2034	0.014	231003
545	*G*030.3701 + 00.4129	0.013	231003
546	*G*029.3767 − 00.1393	0.013	231003
547	*G*029.2366 − 00.3039	0.013	221003
548	*G*031.0465 + 00.1522	0.012	231003
549	*G*031.6255 + 00.1417	0.012	231003
550	*G*033.9410 + 00.3822	0.013	301003
551	*G*033.3780 − 00.3974	0.014	301003
552	*G*034.3524 + 00.0414	0.014	301003
553	*G*034.4886 + 00.0030	0.014	301003
554*[d]	*G*035.1766 − 00.1296	0.012	021103
555	*G*035.8117 + 00.1731	0.011	021103
556	*G*036.6828 + 00.4850	0.009	021103
557	*G*035.3035 − 00.3060	0.012	021103
558	*G*036.5733 + 00.2658	0.011	021103
559	*G*035.7171 − 00.3353	0.009	021103
560	*G*038.9702 + 00.2921	0.012	021103
561	*G*039.0025 + 00.0971	0.012	021103
562	*G*040.3720 + 00.0615	0.011	021103
563	*G*040.8270 − 00.4366	0.011	021103
564	*G*042.6920 − 00.0883	0.015	031103
565	*G*042.8776 − 00.1158	0.015	031103
566	*G*043.3079 − 00.1290	0.015	031103
567	*G*043.3686 − 00.3254	0.015	031103
568*[a]	*G*045.0643 − 00.1249	0.014	031103
569	*G*048.1911 + 00.4459	0.017	031103
570	*G*048.1018 + 00.3077	0.017	031103
571	*G*048.1924 − 00.0121	0.017	031103
441*	*G*029.5298 + 00.0110	0.013	231003
444*[c]	*G*029.6750 − 00.3521	0.013	231003

Notes. (∗) Alias: 534 = ISOGAL − PJ183220.6 − 094910; 535 = [NGM2010] S13; 441=[MHS2002]441; 444=[MHS2002] 444/[MZM2016]68; 554=IRAS 18534+0152; 568=ISOGAL − PJ191416.8 − 104318. (*a*) Stars #534 and #568 (non-detections) are reported as candidate YSOs by Felli et al. (2002). (*b*) Star #535 is a candidate RSG ([NGM2010]S13) in the cluster Alicante 8 (Negueruela et al. 2010). (*c*) Star #444 corresponds to MZM2016-68, an M2I (Messineo et al. 2016). (*d*) For star #554 (IRAS 18534+0152) there is an IRAS low resolution spectrum (LRS, featureless (F), Kwok et al. 1997).

vations. The quoted errors in Table 1 are the errors of the analytic fit with a Gaussian function. As expected, the broader lines are predominantly detected at lower antenna temperatures. By comparing the new sample with the old (Messineo et al. 2002), there is an excess of broader lines between 10° and 50° of longitudes. 14% of masers located at longitudes > 20° has broader lines, but only 5% with longitudes < 20°. Between longitudes 25° and 35°, at the near-end side of the bar, there is a concentration of massive starburst clusters and those are rich in RSG stars (e.g., Messineo et al. 2016, and references therein). A small excess contamination of RSGs is therefore expected at these longitudes (see Appendix C). The nature of objects with apparently broader lines is discussed in Appendix B.

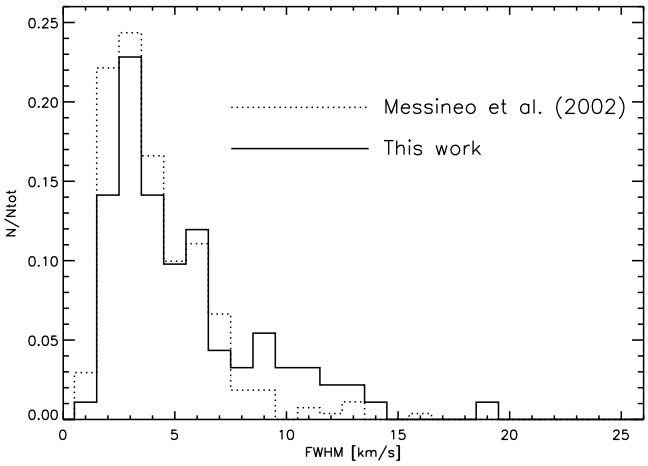

Fig. 2. Histogram of the SiO maser line widths. The solid line shows the distribution of the SiO masers presented in this work; the dotted line those previously published by Messineo et al. (2002). The numbers have been scaled to the total number (444) in the previous study and to the number 135 in the present study

5. Infrared color diagnostics

Because of their low latitudes and low fluxes, the targets have upper limits at 60 μm and the classical IRAS color-color diagram cannot be used to characterise their envelopes (Sect. 6 of Messineo et al. 2004). Sevenster (2002) derived useful diagnostics for OH/IR stars by analysing the MSX colors $[A] - [C]$ and $[D] - [E]$. In the plane defined $D - E$ versus $A - C$ (Fig. 3 of Sevenster 2002), objects of different evolutionary status reside in different areas in the diagram. OH/IR stars reside in the area $A - C < 1.8$ mag and $D - E < 1.5$ mag (Quadrant III); planetary nebulae (PNe) and post-AGB stars (objects in transition to PNe) populate the area $D - E > 1.5$ mag (Quadrants I and II). Our old and new targets are plotted in Fig. 3 in such a diagram, together with known post-AGB stars and PNe from Ortiz et al. (2005). As expected, almost all of our objects are located in Quadrant III, which is the classical region of AGB stars. Only two targets are located in Quadrant II and could have left the AGB already: the SiO emitter #53 and the non-detection #331.

We carefully inspected the quality of measurements and visually inspected the mid-infrared images of these candidate post-AGBs (see Fig. 4). Despite the good flags in the MSX bands both appear located in the halo of a nearby bright 20 μm source, indicating a questionable photometric measurement. We conclude therefore that a contamination of our sample with post-AGB stars and PNe is negligible.

Color-color diagrams can be used also to search for different chemistry in our sample. Ortiz et al. (2005) showed that carbon stars can be identified in a 2MASS-MSX $A - D$ versus $K_s - A$ diagram. In Fig. 5, we show such a diagram with our targets from Table 3 together with carbon stars, post-AGB stars, and PNe from Ortiz et al. (2005). There are ten candidate *C*-rich stars in our sample, #223, #403, #407, #424, #436, #439, #443, #520, #556, and #568, which fall below the separation line dividing *O*-rich and *C*-rich stars in Fig. 5. Two stars, #223 and #520, are masing at 86 GHz indicating an *O*-rich chemistry. Indeed, #520 is also observed by AKARI and has a [9] − [18] color typical of *O*-rich stars (Ishihara et al. 2011). We conclude that the non-

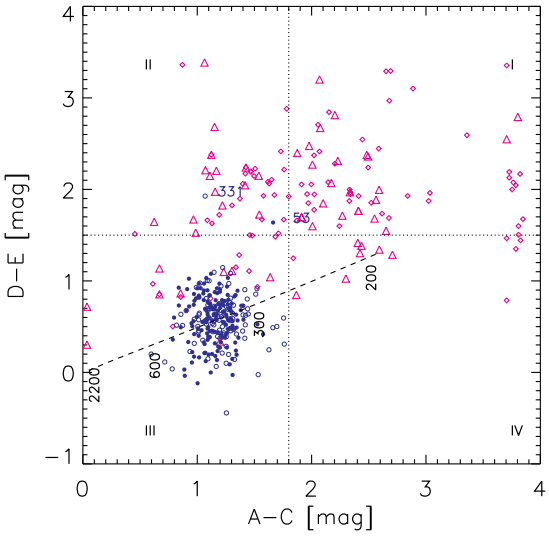

Fig. 3. Diagram of targeted stars in the MSX $A-C$ versus $D-E$ colors. Upper limits and blends have been removed. Targets are marked with blue filled circles (detections) and empty circles (non-detections). As illustration we plot also the positions of astrophysically related objects. Triangles indicate the location of the PNe and diamond symbols that of post-AGB (transitional) objects provided by Ortiz et al. (2005). The long-dashed line marks the locus of a blackbody (F_ν) with a temperature from 2200 K to 200 K.

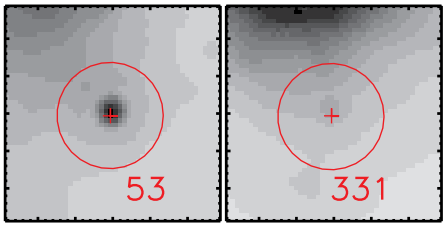

Fig. 4. MIPSGAL 24 μm $1' \times 1'$ maps of the two targets located in Quadrant II of Fig. 3. Images have been bytescaled with a minimum at zero and a maximum at 500 MJy/sr (#53) or 1900 MJy/sr (#331). North is up and east to the left. The IRAM pointing positions are marked with circles of radius $14\farcs5$. The final retained 2MASS positions are marked with crosses.

simultaneity of the near-infrared and mid-infrared measurements yields some spurious C-rich stars.

6. Summary

We have reported on 92 SiO maser detections at 86 GHz, which were made with the IRAM 30-m single dish in 2003. This dataset along with the 271 detections by Messineo et al. (2002) was used as probe of the Galactic barred potential in the work by Habing et al. (2006). The 2003 detections are located between 20° and 50° of longitude, and yield a detection rate of 68%, similar to that reported by Messineo et al. (2002). Since no archival copy exists of this dataset, here, we make them available.

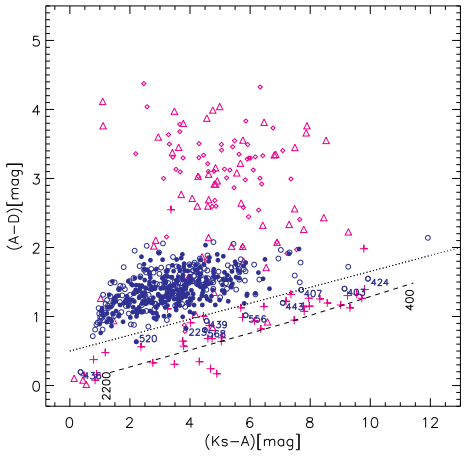

Fig. 5. 2MASS-MSX K_s-A versus $A-D$ diagram of targets. SiO maser detections are marked with blue filled circles and non-detections with blue empty circles. Upper limits and blends have been removed. Identification numbers are as in Table 3. The dotted line marks the separation between O-rich and C-rich shells found by Ortiz et al. (2005). The long-dashed line represents a blackbody (F_ν) with temperature from 2200 to 400 K. New candidate C-type stars from our survey (see text) are labeled. For comparison K_s-A versus $A-D$ values of the carbon stars analyzed by Ortiz et al. (2005) are overplotted with magenta crosses, transitional objects with diamonds, and PNe with triangles.

We performed identifications of the 135 targets presented in this work and of the 444 of Messineo et al. (2002) in the MSX, WISE, MIPSGAL, GLIMPSE, 2MASS, DENIS, ISOGAL and AKARI catalogs. The sample is made of Mira-like stars, and a fraction of 74% of stars shows photometric variability in at least one of the band.

We used the collected measurements to confirm their O-rich nature, as initially designed. For example, we analyze the $A-D$ versus K_s-A diagram to separate O- and C-rich stars, and found 1.7% of them could be C-rich stars. The $D-E$ versus $A-C$ plane allows us to separate normal AGB stars from post-AGB stars and PNe. Only one masing star, #53, is marginally deviating from the locus of normal AGB stars in this diagram.

Acknowledgements. IRAM is supported by INSU/CNRS (France), MPG (Germany) and IGN (Spain). ISOGAL is based on observations with ISO, an ESA project with instruments funded by ESA Member States (especially the PI countries: France, Germany, the Netherlands and the United Kingdom) and with the participation of ISAS and NASA. DENIS is a joint effort of several Institutes mostly located in Europe. It has been supported mainly by the French Institut National des Sciences de l'Univers, CNRS, and French Education Ministry, the European Southern Observatory, the State of Baden-Wuerttemberg, and the European Commission under networks of the SCIENCE and Human Capital and Mobility programs, the Landessternwarte, Heidelberg and Institut d'Astrophysique de Paris. This publication makes use of data products from the Two Micron All Sky Survey, which is a joint project of the University of Massachusetts and the Infrared Processing and Analysis Center/California Institute of Technology, funded by the National Aeronautics and Space Administration and the National Science Foundation. This work is based on observations made with the Spitzer Space Telescope, which is operated by the Jet Propulsion Laboratory, California Institute of Technology under a contract with NASA. This research made use of data products from the Midcourse Space Experiment, the processing of which was funded by the Ballistic Missile Defence Organization with additional support from the NASA Office of Space Science. This publication makes use of data products from WISE, which is a joint project of the University of California, Los Angeles, and the Jet Propulsion Laboratory/California Insti- tute of Technology, funded

by the National Aeronautics and Space Administration. This work is based in part on data obtained as part of the UKIRT Infrared Deep Sky Survey. This research has made use of the SIMBAD data base, operated at CDS, Strasbourg, France. This research made use of Montage, funded by the National Aeronautics and Space Administration's Earth Science Technology Office, Computational Technnologies Project, under Cooperative Agreement Number NCC5-626 between NASA and the California Institute of Technology. The code is maintained by the NASA/IPAC Infrared Science Archive. AKARI is a JAXA project with the participation of the European Space Agency (ESA). The work of MM from 2000 to 2004 was funded by the Netherlands Research School for Astronomy (NOVA) through a network 2 Ph.D. stipend. We thank Dr. Sevenster M. N. for stimulating discussion on Galaxy morphology and masing stars; she was a visiting fellow of the Leiden Observatory from 2002 to 2004. This work was partially supported by the Fundamental Research Funds for the Central Universities in China, and USTC grant KY2030000054. The National Radio Astronomy Observatory is a facility of the National Science Foundation operated under cooperative agreement by Associated Universities, Inc. We thank the referees of this paper.

References

Alcolea, J., Bujarrabal, V., & Gomez-Gonzalez, J. 1990, A&A, 231, 431
Alcolea, J., Pardo, J. R., Bujarrabal, V., et al. 1999, A&AS, 139, 461
Benjamin, R. A., Churchwell, E., Babler, B. L., et al. 2003, PASP, 115, 953
Blommaert, J. A. D. L., van Langevelde, H. J., & Michiels, W. F. P. 1994, A&A, 287, 479
Cabrera-Lavers, A., Garzón, F., Hammersley, P. L., Vicente, B., & González-Fernández, C. 2006, A&A, 453, 371
Churchwell, E., Babler, B. L., Meade, M. R., et al. 2009, PASP, 121, 213
Clark, J. S., Negueruela, I., Davies, B., et al. 2009, A&A, 498, 109
Cutri, R. M. & et al. 2013, VizieR Online Data Catalog, 2328
Debattista, V. P., Gerhard, O., & Sevenster, M. N. 2002, MNRAS, 334, 355
Deguchi, S., Fujii, T., Glass, I. S., et al. 2004, PASJ, 56, 765
Deguchi, S., Fujii, T., Izumiura, H., et al. 2000a, ApJS, 130, 351
Deguchi, S., Fujii, T., Izumiura, H., et al. 2000b, ApJS, 128, 571
Deguchi, S., Fujii, T., Izumiura, H., et al. 2000c, ApJS, 130, 351
Deguchi, S., Nakashima, J.-I., Zhang, Y., et al. 2010, PASJ, 62, 391
Egan, M. P., Price, S. D., Kraemer, K. E., et al. 2003, VizieR Online Data Catalog, 5114
Egan, M. P., Price, S. D., Moshir, M., et al. 1999, Air Force Research Lab. Technical Rep. AFRL-VS-TR-1999-1522 (1999)
Epchtein, N., de Batz, B., Copet, E., et al. 1994, Ap&SS, 217, 3
Felli, M., Testi, L., Schuller, F., & Omont, A. 2002, A&A, 392, 971
Gutermuth, R. A. & Heyer, M. 2015, AJ, 149, 64
Habing, H. J., Sevenster, M. N., Messineo, M., van de Ven, G., & Kuijken, K. 2006, A&A, 458, 151
Halpern, J. P. & Gotthelf, E. V. 2007, ApJ, 669, 579
Iben, I. & Renzini, A. 1983, ARA&A, 21, 271
Ishihara, D., Kaneda, H., Onaka, T., et al. 2011, A&A, 534, A79
Ishihara, D., Onaka, T., Kataza, H., et al. 2010, A&A, 514, A1
Izumiura, H., Deguchi, S., Fujii, T., et al. 1999, ApJS, 125, 257
Jura, M. & Kleinmann, S. G. 1990, ApJS, 73, 769
Kwok, S., Volk, K., & Bidelman, W. P. 1997, ApJS, 112, 557
Le Bertre, T. & Nyman, L.-A. 1990, A&A, 233, 477
Lindqvist, M., Winnberg, A., Habing, H. J., & Matthews, H. E. 1992, A&AS, 92, 43
López-Corredoira, M., Garzón, F., Beckman, J. E., et al. 1999, AJ, 118, 381
Lucas, P. W., Hoare, M. G., Longmore, A., et al. 2008, MNRAS, 391, 136
Messineo, M., Habing, H. J., Menten, K. M., Omont, A., & Sjouwerman, L. O. 2004, A&A, 418, 103
Messineo, M., Habing, H. J., Menten, K. M., et al. 2005, A&A, 435, 575
Messineo, M., Habing, H. J., Sjouwerman, L. O., Omont, A., & Menten, K. M. 2002, A&A, 393, 115
Messineo, M., Zhu, Q., Menten, K. M., et al. 2016, ApJ, 822, L5
Messineo, M., Zhu, Q., Menten, K. M., et al. 2017, ApJ, 836, 65
Nagata, T., Hyland, A. R., Straw, S. M., Sato, S., & Kawara, K. 1993, ApJ, 406, 501
Negueruela, I., González-Fernández, C., Marco, A., & Clark, J. S. 2011, A&A, 528, A59
Negueruela, I., González-Fernández, C., Marco, A., Clark, J. S., & Martínez-Núñez, S. 2010, A&A, 513, A74
Omont, A., Gilmore, G. F., Alard, C., et al. 2003, A&A, 403, 975
Ortiz, R., Lorenz-Martins, S., Maciel, W. J., & Rangel, E. M. 2005, A&A, 431, 565
Reid, M. J., Menten, K. M., Zheng, X. W., et al. 2009, ApJ, 700, 137
Schuller, F., Ganesh, S., Messineo, M., et al. 2003, A&A, 403, 955
Sevenster, M. N. 1999, MNRAS, 310, 629
Sevenster, M. N. 2002, AJ, 123, 2772
Sevenster, M. N., Chapman, J. M., Habing, H. J., Killeen, N. E. B., & Lindqvist, M. 1997a, A&AS, 122
Sevenster, M. N., Chapman, J. M., Habing, H. J., Killeen, N. E. B., & Lindqvist, M. 1997b, A&AS, 124
Sevenster, M. N., van Langevelde, H. J., Moody, R. A., et al. 2001, A&A, 366, 481
Sjouwerman, L. O., van Langevelde, H. J., Winnberg, A., & Habing, H. J. 1998, A&AS, 128, 35
Skrutskie, M. F., Cutri, R. M., Stiening, R., et al. 2006, AJ, 131, 1163
Verheyen, L., Messineo, M., & Menten, K. M. 2012, A&A, 541, A36
Wright, E. L., Eisenhardt, P. R. M., Mainzer, A. K., et al. 2010, AJ, 140, 1868
Yamamura, I., Makiuti, S., Ikeda, N., et al. 2010, VizieR Online Data Catalog, 2298

Appendix A: Spectra

The spectra of targets with detected SiO maser are shown in Fig. A.1.

Appendix B: Notes to the infrared catalogs

2MASS matches were provided by the two catalogs WISE and GLIMPSE. We generally adopted the AllWISE Data Release, which has an improved astrometry, but, the number of targets was in only the earlier WISE All-Sky Data Release. When 2MASS matches were missed by GLIMPSE (mostly due to saturation effects), we inspected the images (GLIMPSE, WISE, and 2MASS) and retained the WISE matches. We inspected the images and retained the GLIMPSE values when 2MASS matches had been missed by WISE (mostly due to saturation effects and crowding). We retained the 2MASS matches provided by GLIMPSE for targets #58, #78, #320, #342, and #493. One near-infrared star (#39) is resolved by UKIDSS into two similarly bright stars. UKIDSS data were used to revise the positions and magnitudes of #58, #320, and #413 because they were blended or missed in 2MASS. We assigned UKIDSS magnitudes for four entries without 2MASS data (#224, #298, #423, and #536).

In Messineo et al. (2004) 2MASS, ISOGAL, and MSX (v1.2) counterparts have already been provided for the 444 stars in Messineo et al. (2002). The MSX magnitudes tabulated in this paper differ from those in Messineo et al. (2004) because there we used an earlier version of the MSX catalog. We compared the K_s measurements listed by Messineo et al. (2004) with those in Table 3 and found only five 2MASS mismatches (targets #77, #90, #227, #347, and #424) and the updated seven K_s values with measurements from the UKIDSS catalog. Masers #77 and #78 were detected in the same beam. The maser with the stronger flux was associated with the pointed star ISOGAL−J174618.9-284439. The fainter maser #77 had been included in Messineo et al. (2004) and had been associated with the only star detected at #7 μm by ISOGAL about 12.″5 away. The GLIMPSE catalog allows us to revise this association with the closer GLIMPSE star G000.2444−00.0294 (5.″2 away, [8.0]=4.93 mag and K_s=7.78 mag). Stars #21 and #22 are double detections within the same pointing, identified with two ISOGAL point sources. The two masers #64 and #65 were both detected when pointing toward the mid-infrared source ISOGAL−J174528.8-284734. Possible fainter stars ($\approx$ 8 mag) falling in the IRAM beam are detected in the 8 μm GLIMPSE images; however, they are below [8.0]= 8.0 mag, while the average brightness of our SiO masing stars is [8.0]= 4.2 mag with a σ=0.6 mag.

The WISE counterparts were searched within 10″, and the closest was retained. We found 28 cases of multiple stars within the search radius. The closest match was the brightest in the

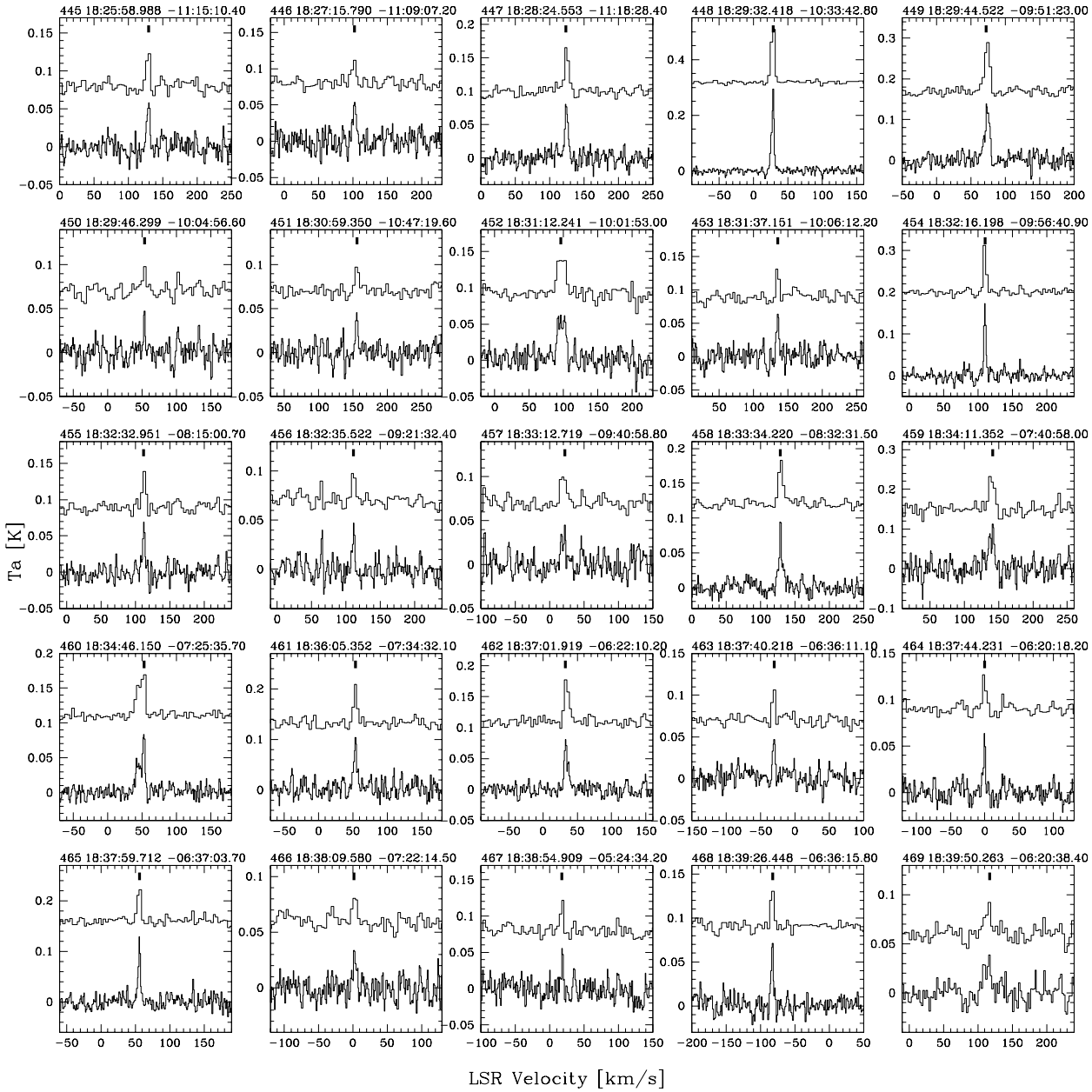

Fig. A.1. IRAM spectra of 86 GHz SiO maser lines. Each panel shows at the bottom the spectrum obtained with the autocorrelator (1.1 km s^{-1}), and at the top that obtained with the filter bank (3.5 km s^{-1}, offset from zero). The line-of-sight velocity listed in Table 1 is indicated with a small vertical bar at the top of each panel. The conversion factor between antenna temperatures and flux densities is 6.2 Jy/K.

$W3$ band in all cases but #110 and #405. The reddest K_s-W3 match was not the closest in the cases of stars #21 (9.4″ away), #35 (6.7″ away), #43 (9.7″ away), #110 (8.0″ away), #173 (6.″6 away) #207 (7.″8 away), #228 (6.″1 away), #289 (9.″5 away), #324 (4.″4 away), #354 (4.″7 away), #405 (9.″1 away), #479 (9.″8 away), #482 (9.″8 away), #502 (9.″6 away), #545 (8.″3 away), and #548 (8.″7 away). We searched for AKARI/FIS data at 65, 90, and 140 μm (Yamamura et al. 2010), but, unfortunately, matches were available only for three targets (#251, #451, and #537).

Appendix C: Contamination RSGs

To asses the nature of a few suspect broad and multipeaked maser lines, which are reported in Sect. 4.2, we estimated luminosities and distances. Extinction corrections are as in Messineo et al. (2005). Bolometric magnitudes were computed by integrating the dereddened flux densities, $F_\nu(\nu)$ over frequency ν with linear interpolations and by extrapolating to $F_{\nu=0} = 0$ and at the upper end with a blackbody curve. The

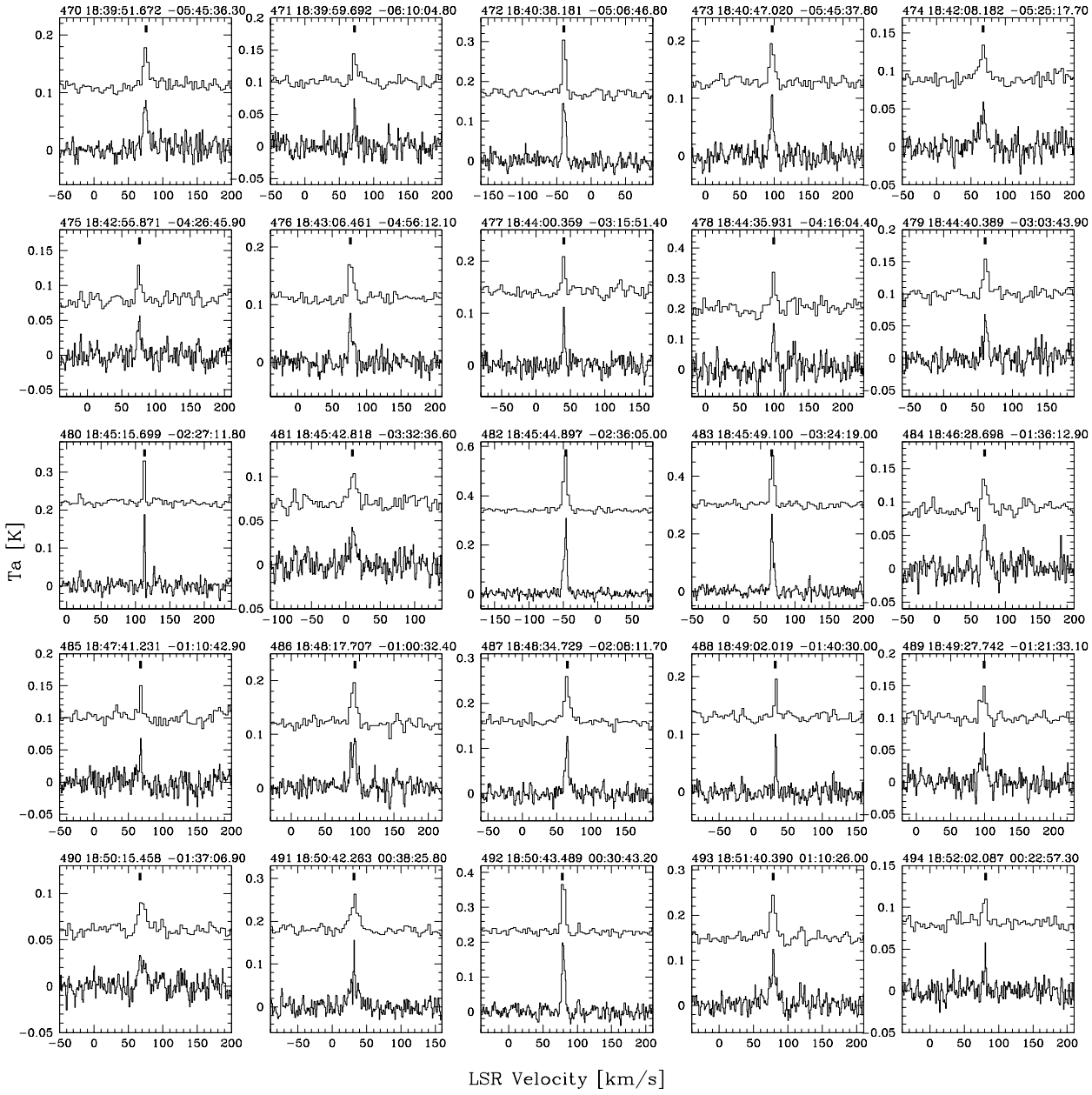

Fig. A.1. Continuation of Fig. A.1.

low-frequency extrapolation is insignificant since it contains a negligible fraction of the total flux (3% in average). When both DENIS and 2MASS datasets were available, we averaged the two estimates to attenuate the effect of variability; the average difference being 0.036 mag with $\sigma = 0.31$ mag.

In Table C.1, we list M_{bol} values of the brighest stars. The list is useful because it contains probable RSG stars, but infrared spectroscopy is needed to firmly unveil the nature of those bright stars. The Table collects the brighest stars from five computations with different assumptions on distances.

Group 1: Previously known RSGs included in the sample.

Group 2: Stars located in the central 5° of longitude which are brighter than the AGB limit, $M_{\rm bol} < -7.2$ mag, when a distance modulus of 14.5 mag is assumed.
Group 3: Brighest stars with longitude > 20° for which kinematic near distances are used.
Group 4: Brighest stars with longitude < 20° and classified as foreground to the bar and bulge in Messineo et al. (2005). For these stars, kinematic distances are assumed.
Group 5: List of all remaining targets with FWHM > 9 km s^{-1}.

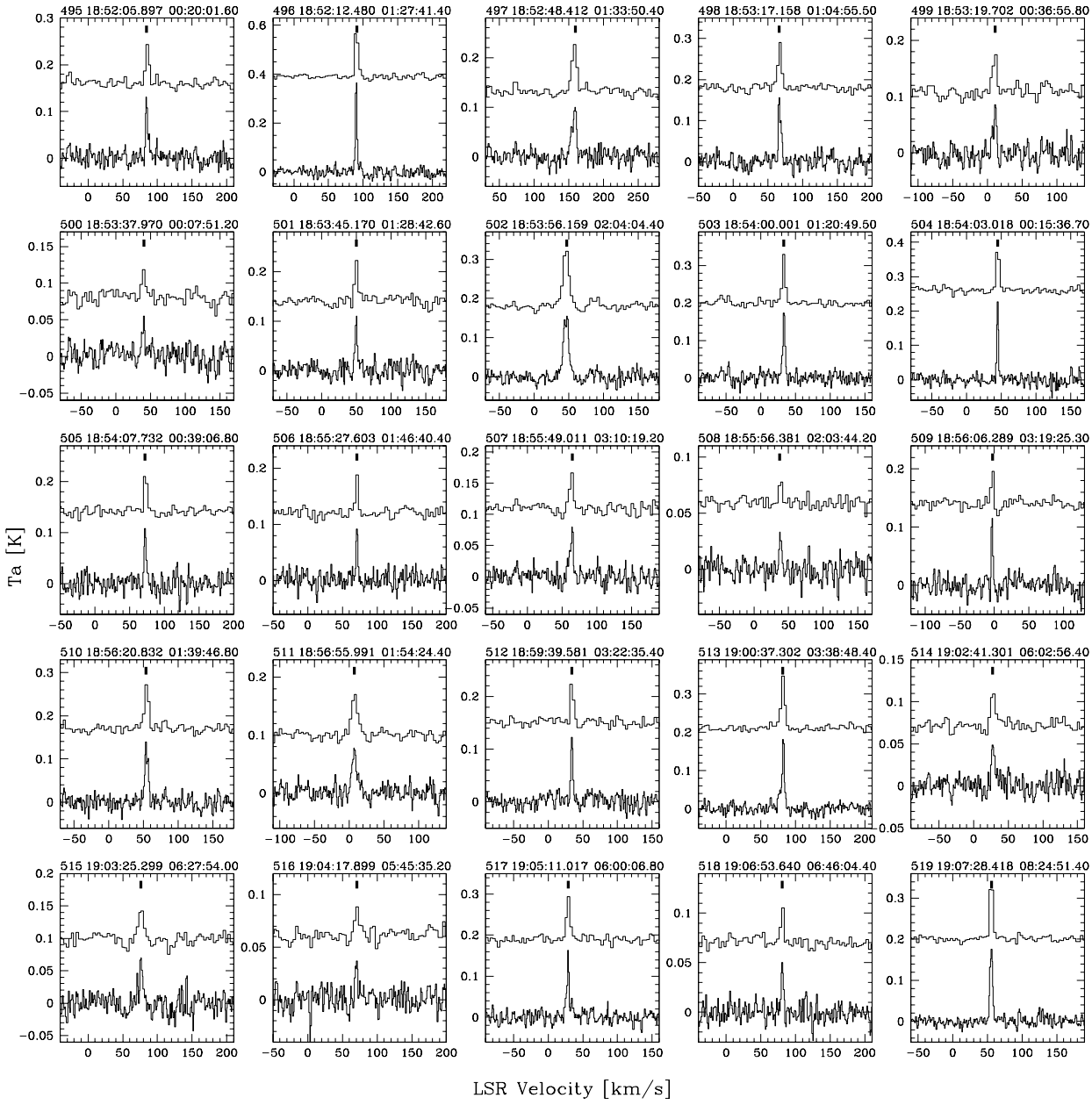

Fig. A.1. Continuation of Fig. A.1.

Group 1 : The sample contains two spectroscopically identified RSGs, #436 and #444 (Jura & Kleinmann 1990; Messineo et al. 2017), and two photometrically identified RSGs, #483 and #535 (Clark et al. 2009; Negueruela et al. 2010). Only star #483 (l=29°) is a maser detection; it has a velocity $V_{\rm lsr}$=66.89 km s^{-1}, and M_{bol}=−5.63 mag.

Group 2 : For the 251 targets located within the inner 5° in longitude, we initially assume a distance of 8.0 kpc. The bulk of targets have $M_{\rm bol}$ from −4.5 to −6.0 mag as expected for thermally pulsing AGB stars. A bright tail in the luminosity distribution suggests that a few RSGs are included in the sample. A number of 17 stars (7% of targets within 5°) are brighter than $M_{\rm bol}$ = −7.2 mag, which is the classical AGB limit (Iben & Renzini 1983). Ten of them are likely to be foreground stars, because their total extinction is lower than the average interstellar extinction of surrounding stars (Messineo et al. 2005). The remaining seven bright sources (#31, #75, #92, #116, #128, #294, and #310) with average $M_{\rm bol} < -7.2$ mag have total extinction very close to that measured from surrounding stars, therefore, M_{bol} does not depend on the choice of A_{K_s}. For stars, #31, #92, #128, and #294, infrared spectra are analyzed in the work by Messineo et al. (2017). Stars #31 (M_{bol}(2MASS)=−7.47 and M_{bol}(DENIS)=−7.17 mag) and #128 (M_{bol}(2MASS)=−7.94 and M_{bol}(DENIS)= −6.49 mag) have some water absorption which

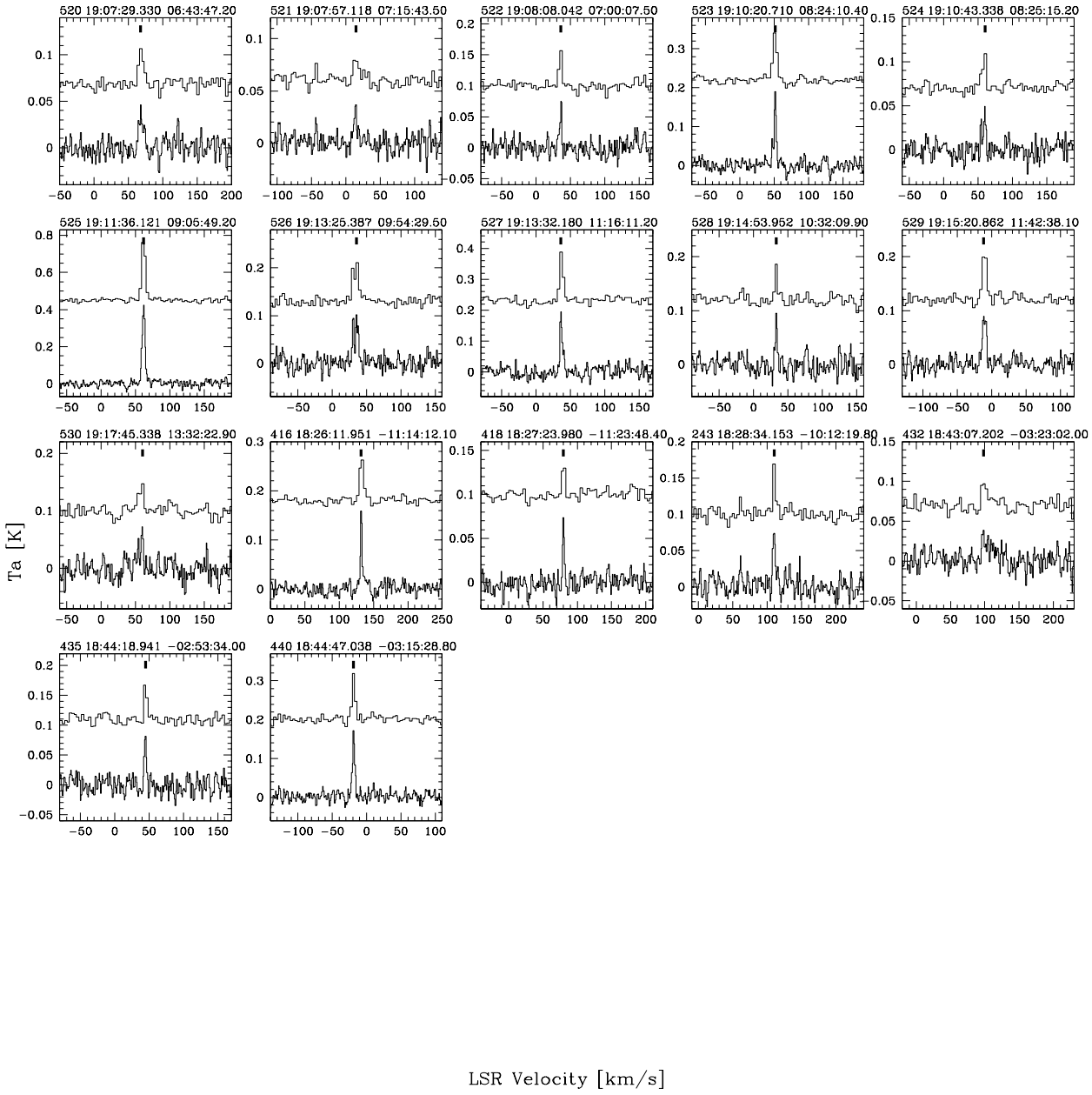

Fig. A.1. Continuation of Fig. A.1.

suggests AGB stars. Stars #92 and #294 have a low water content and broad CO bands that are typical of RSGs. Their M_{bol}(2MASS) are −8.22 and −7.76 mag. Star #92 ($V_{\rm lsr}$=119 km s^{-1}) is already classified as a RSG by Nagata et al. (1993) and Messineo et al. (2017).

Group 3 : Using kinematic distances (Reid et al. 2009), their M_{bol} values do not exceed the AGB limit. We note that in *Group 2* most of the stars have $M_{\rm bol}$ from −4.5 to −6.0 mag. We are able to locate eight bright stars at $l > 20^\circ$ with $M_{bol} < -6.0$ mag (i.e., 7% of detections at $l > 20^\circ$).

Group 4 : Stars defined as foreground by Messineo et al. (2005) may include some RSGs. Their A_{K_s} values is smaller than that of the average of surrounding stars. Indeed, M_{bol} estimated for stars #15 and #129 approach the AGB limit.

Group 5 : Most of the remaining stars with FWHMs > 9 km s^{-1} have M_{bol} values larger than −5.5 mag. We estimate that the RSG contamination is $\lesssim$ 7% (Table C.1). With our signal-to-noise it is not possible to use the FWHM of maser lines to establish luminosity classes; however, candidate RSGs have in average broader lines. For example, at $l > 20^\circ$ 15% of the detections have broad FWHMs (> 9 km s^{-1}), but only 7% of the detections are candidate RSGs (25% of which have FWHMs > 9 km s^{-1}).

Table C.1. Luminosities of bright targets and of targets with broad maser lines.

ID	Long [°]	A_K(field) [mag]	A_K(tot) [mag]	M_{bol}(kin) [mag]	M_{bol}(14.5) [mag]	$V_{\rm lsr}$ [km s^{-1}]	FWHM [km s^{-1}]	Comments	References
436	29.85	0.12	..0	..	−8.4	..	..	M3I	(1)
444	29.67	1.16	0.88	..	−7.9	..	..	M2I	(2)
483	29.26	1.32	1.40	−5.6	−7.1	66.9	4.3	RSG[a]	(3)
535	24.63	1.29	1.76	..	−5.0	..	..	RSG[a]	(4)
31	−0.44	1.80	1.72	..	−7.3	−24.4	9.6	M_{bol}(14.5)<-7.2, long< 5°	
75	0.77	1.36	1.20	..	−8.0	−38.1	3.3	M_{bol}(14.5)<-7.2, long< 5°	
92	0.11	1.66	1.41	..	−8.2	119.4	2.9	M_{bol}(14.5)<-7.2, long< 5°, sRSG[b]	(5)
116	2.49	1.75	1.40	..	−7.6	19.5	4.2	M_{bol}(14.5)<-7.2, long< 5°	
128	2.70	1.51	1.60	..	−7.9	−16.4	4.5	M_{bol}(14.5)<-7.2, long< 5°	
294	−1.00	2.23	2.37	..	−7.8	..	..	M_{bol}(14.5)<-7.2, long< 5°, sRSG[b]	(5)
310	−0.55	2.79	2.42	..	−7.4	..	..	M_{bol}(14.5)<-7.2, long< 5°	
244	20.40	0.96	0.99	−6.2	−7.1	89.1	3.3	M_{bol}(kin)< −6.0, long> 20°	
449	21.70	1.05	0.91	−6.3	−7.6	73.6	8.2	M_{bol}(kin)< −6.0, long> 20°	
456	22.46	1.61	1.36	−6.6	−7.3	111.1	3.5	M_{bol}(kin)< −6.0, long> 20°	
460	24.43	1.20	0.98	−6.2	−8.1	49.0	13.2	M_{bol}(kin)< −6.0, long> 20°	
473	26.59	0.72	0.65	−6.1	−7.0	96.8	6.0	M_{bol}(kin)< −6.0, long> 20°	
474	27.05	0.82	0.50	−6.4	−7.9	66.9	11.8	M_{bol}(kin)< −6.0, long> 20°	
484	30.94	0.56	0.35	−6.3	−7.7	69.2	7.3	M_{bol}(kin)< −6.0, long> 20°	
495	33.30	0.95	0.59	−6.1	−7.1	84.5	3.8	M_{bol}(kin)< −6.0, long> 20°	
15	−1.38	0.99	0.89	−6.9	−7.2	38.7	7.3	M_{bol}(kin)< −6.0, long< 20°, FG[c]	
23	−1.29	1.22	1.07	−6.8	−7.0	56.5	2.8	M_{bol}(kin)< −6.0, long< 20°, FG[c]	
113	1.98	1.31	1.13	−6.7	−7.1	31.7	13.9	M_{bol}(kin)< −6.0, long< 20°, FG[c]	
129	3.82	0.47	0.36	−7.1	−7.7	38.0	13.9	M_{bol}(kin)< −6.0, long< 20°, FG[c]	
130	4.49	0.68	0.52	−6.4	−6.9	52.8	3.2	M_{bol}(kin)< −6.0, long< 20°, FG[c]	
160	6.96	0.82	0.82	−6.2	−7.3	39.9	7.8	M_{bol}(kin)< −6.0, long< 20°, FG[c]	
71	0.32	1.84	2.12	..	−5.3	92.5	9.0	remaining FWHM > 9	
87	1.24	1.21	1.24	..	−7.2	−15.3	9.2	remaining FWHM > 9	
117	2.01	1.85	3.25	..	−5.6	22.2	16.3	remaining FWHM > 9	
135	3.81	1.20	1.46	..	−5.6	207.1	11.9	remaining FWHM > 9	
173	8.66	1.61	1.20	..	−7.5	−1.1	11.5	remaining FWHM > 9	
190	10.99	1.04	1.10	..	−6.4	58.1	9.1	remaining FWHM > 9	
203	14.31	0.91	3.14	..	−4.0	81.1	12.7	remaining FWHM > 9	
223	17.80	1.02	1.87	..	−5.2	143.9	13.4	remaining FWHM > 9	
232	17.92	1.10	1.45	..	−5.4	94.3	9.8	remaining FWHM > 9	
452	21.71	1.11	1.54	−5.7	−6.6	97.1	13.3	remaining FWHM > 9	
457	22.25	1.51	1.28	−4.3	−7.5	19.8	9.1	remaining FWHM > 9	
459	24.13	1.05	1.66	−5.5	−5.6	139.5	10.4	remaining FWHM > 9	
469	25.97	0.86	1.70	−4.3	−4.9	113.4	12.7	remaining FWHM > 9	
481	29.12	0.73	0.31	−3.2	−7.8	10.2	11.7	remaining FWHM > 9	
486	31.67	1.75	5.20	−4.2	−5.2	91.0	10.6	remaining FWHM > 9	
489	31.50	1.43	2.68	−4.7	−5.4	98.0	9.8	remaining FWHM > 9	
490	31.36	1.55	2.27	−4.0	−5.5	69.8	12.4	remaining FWHM > 9	
491	33.42	1.11	1.09	−4.2	−7.0	31.5	14.6	remaining FWHM > 9	
493	34.00	1.04	1.38	−5.0	−6.1	78.9	11.1	remaining FWHM > 9	
502	35.06	2.02	2.02	−5.4	−7.5	45.8	9.1	remaining FWHM > 9	
511	35.25	1.47	2.49	−0.9	−6.2	7.3	9.2	remaining FWHM > 9	
526	44.24	0.94	1.39	−3.2	−5.7	34.0	9.7	remaining FWHM > 9	
530	47.95	0.71	1.88	−4.0	−4.8	58.0	10.4	remaining FWHM > 9	
432	28.97	0.97	1.17	−5.4	−6.2	103.1	19.9	remaining FWHM > 9	

Notes. Identification numbers (ID) are followed by longitudes (Long), median extinction of surrounding stars A_K(field), total extinction of the targets A_K(tot) (Messineo et al. 2005), M_{bol} values obtained by adopting the near kinematic distances, M_{bol}(kin), M_{bol} values obtained by adopting a distance modulus of 14.5 mag, radial velocities, $V_{\rm lsr}$, and the maser line FWHMs.

References. 1=Jura & Kleinmann (1990) ; 2= Messineo et al. (2016); 3=Clark et al. (2009); 4=Negueruela et al. (2010); 5= this work.

[a] RSG = Star photometrically reported as a probable RSG in previous studies.

[b] sRSG = Stars confirmed as RSGs in this work with the spectral indexes of Messineo et al. (2017).

[c] FG = Stars classified as likely foreground by Messineo et al. (2005), their $A_{K_{\rm s}}$ values are smaller than the average $A_{K_{\rm s}}$ of surrounding stars.

Table 3. Infrared measurements of the targeted stars**

	2MASS		DENIS-ISOGAL								GLIMPSE				MSX				WISE				MIPS	AKARI		Nstar+
ID	RA(J2000)	DEC(J2000)	*J*	*H*	K_S	*I*	*J*	K_S	[7]	[15]	[3.6]	[4.5]	[5.8]	[8.0]	*A*	*C*	*D*	*E*	*W1*	*W2*	*W3*	*W4*	[24]	[9]	[18]	
			1.2	1.6	2.2	0.8	1.2	2.2	7	15	3.6	4.5	5.8	8.0	8.3	12.1	14.6	21.3	3.4	4.6	11.6	22.1	23.7	9.0	18.0	
			[mag]	[mag]	[mag]	[mag]	[mag]	[mag]	[mag]	[mag]	[mag]	[mag]	[mag]	[mag]	[mag]	[mag]	[mag]	[mag]	[mag]	[mag]	[mag]	[mag]	[mag]	[mag]	[mag]	
1	17 31 40.98	−32 03 55.94	12.53	9.66	8.10	..	12.77	8.28	5.16	3.48	6.93	6.98	5.74	5.16	5.30	98.98	98.98	98.98	94.94	94.94	4.74	3.33	2.58	96.96	2.94	111
2	17 36 42.18	−30 59 11.74	14.67	10.42	8.09	..	14.92	8.16	4.89	3.06	88.88	88.88	88.88	88.88	3.80	2.87	2.27	1.55	6.45	5.03	3.42	1.76	1.92	3.77	2.71	111
3	17 37 07.29	−31 21 31.29	12.42	9.30	7.60	94.94	12.22	7.53	4.99	3.55	88.88	88.88	88.88	88.88	4.86	98.98	98.98	98.98	6.19	5.25	3.97	2.75	2.97	4.64	3.23	111
4	17 37 29.35	−31 17 16.62	(15.41)	10.59	8.08	..	15.01	7.97	4.31	3.44	88.88	88.88	88.88	88.88	4.84	98.98	3.17	98.98	6.55	5.50	4.43	3.17	2.68	4.68	3.57	111
5	17 38 11.78	−31 46 27.03	11.62	8.70	7.02	..	11.78	7.02	96.96	96.96	88.88	88.88	88.88	88.88	3.38	2.23	2.16	98.98	5.15	4.19	2.65	1.50	1.63	3.69	2.19	111
6	17 38 12.49	−29 39 38.53	11.73	9.69	8.29	17.36	11.77	8.06	5.26	2.89	88.88	88.88	88.88	88.88	4.17	3.09	3.13	98.98	8.75	8.71	8.22	98.98	96.96	4.35	3.49	111
7	17 38 17.07	−29 42 32.42	7.75	6.22	5.38	12.65	..	6.42	4.63	3.02	4.62	4.86	4.46	4.21	97.97	97.97	97.97	97.97	4.59	4.35	3.82	3.05	3.33	4.18	96.96	121
8	17 38 29.01	−31 26 17.49	11.01	7.94	6.29	..	10.68	6.85	4.04	2.93	..	5.28	4.48	4.38	4.24	3.08	2.78	98.98	94.94	94.94	3.70	2.48	2.89	3.85	2.37	111
9	17 38 32.50	−31 20 42.75	(14.14)	9.99	7.75	..	13.94	7.67	4.74	3.44	88.88	88.88	88.88	88.88	4.77	3.48	3.47	98.98	5.63	4.88	4.09	3.10	3.23	96.96	3.51	111
10	17 38 35.69	−29 36 37.21	12.58	9.80	8.12	19.15	11.21	7.33	4.59	..	88.88	88.88	88.88	88.88	3.73	2.82	2.43	1.52	6.48	5.32	3.57	1.93	1.16	3.39	1.74	111
11	17 39 37.28	−30 08 51.64	10.02	7.90	6.67	16.94	9.99	6.63	4.57	3.09	88.88	88.88	88.88	88.88	4.24	3.14	3.02	98.98	4.99	4.55	3.34	2.14	2.06	..	..	111
12	17 40 57.23	−29 45 31.45	11.87	8.87	(7.48)	..	11.60	7.16	4.07	2.70	6.71	6.18	5.14	4.46	4.30	3.20	2.80	98.98	7.80	6.50	3.97	2.27	1.94	4.08	2.79	111
13	17 41 16.81	−31 38 10.59	14.04	10.49	8.43	..	13.54	8.30	4.98	3.05	6.79	6.00	5.48	4.79	3.97	2.78	2.53	98.98	6.97	5.42	3.32	1.70	1.50	96.96	2.61	111
14	17 41 26.93	−29 30 46.97	12.00	9.17	7.39	..	11.80	7.39	4.48	3.56	88.88	88.88	88.88	88.88	5.01	98.98	98.98	98.98	5.87	5.07	3.59	2.18	2.86	..	..	191
15	17 41 31.31	−30 00 18.87	7.73	5.73	4.64	16.43	8.61	6.36	3.24	2.03	88.88	88.88	88.88	88.88	3.13	1.97	1.88	98.98	4.34	3.73	2.71	1.92	1.59	..	..	111
16	17 41 36.86	−29 29 30.99	12.69	9.53	7.58	..	12.23	7.06	3.79	2.00	5.42	..	4.59	4.28	3.48	2.41	2.15	1.45	5.86	4.90	2.90	1.47	1.93	..	..	111
17	17 41 37.41	−29 32 05.73	12.18	9.08	7.30	..	12.26	7.37	4.60	2.85	88.88	88.88	88.88	88.88	4.49	3.44	3.07	98.98	5.44	4.50	3.41	2.08	2.51	..	..	111
18	17 42 04.36	−29 58 46.37	13.12	9.88	8.06	..	12.16	7.33	4.83	3.40	6.68	6.35	5.59	5.31	5.26	98.98	98.98	98.98	6.47	5.88	4.79	3.64	3.40	4.97	96.96	111
19	17 42 06.86	−28 18 32.39	9.64	7.89	6.88	15.86	9.59	6.87	4.82	3.12	88.88	88.88	88.88	88.88	4.66	3.57	3.56	3.20	6.14	5.58	3.90	2.55	2.75	4.70	3.54	111
20	17 42 23.28	−29 39 35.57	12.13	9.13	7.46	..	12.52	7.60	5.11	2.95	88.88	88.88	88.88	88.88	4.43	3.29	3.03	98.98	5.85	5.01	3.70	2.27	2.19	4.75	2.83	111
21*	17 42 32.91	−29 41 25.10	11.62	9.15	7.76	17.23	11.78	7.79	..	4.64	6.94	6.47	6.08	5.77	97.97	97.97	97.97	97.97	6.51	6.08	5.46	3.80	3.70	..	..	121
22	17 42 32.48	−29 41 10.73	12.55	9.46	7.67	..	11.94	7.19	4.33	3.08	88.88	88.88	88.88	88.88	97.97	97.97	97.97	98.98	6.54	4.72	3.80	2.24	2.23	96.96	2.61	111
23	17 42 44.87	−30 04 08.08	9.10	6.87	5.67	16.27	8.65	6.40	4.29	2.71	7.21	..	4.42	4.20	4.30	3.36	3.16	98.98	4.98	4.52	3.59	2.82	2.98	..	..	111
24	17 43 09.81	−29 24 03.32	15.54	10.79	8.19	..	14.50	7.53	3.65	1.93	5.29	..	4.11	3.71	3.40	2.12	1.72	1.01	5.03	3.72	2.29	0.79	1.14	96.96	1.55	111
25	17 43 23.46	−28 53 50.33	8.44	6.21	4.97	15.73	8.01	93.93	2.87	2.16	4.05	3.85	3.59	3.20	3.30	2.41	2.13	2.17	3.73	3.13	2.50	1.78	2.10	96.96	2.08	111
26	17 43 25.26	−29 45 28.56	15.88	11.69	9.09	..	15.23	8.99	4.92	2.76	6.80	6.14	5.12	4.55	4.16	2.94	2.58	98.98	94.94	94.94	3.15	1.62	1.43	96.96	2.53	111
27	17 43 32.72	−29 15 39.37	13.34	9.63	7.47	..	12.06	6.91	3.94	2.45	5.37	5.21	4.50	4.18	3.50	2.50	2.33	1.85	94.94	94.94	2.91	1.45	1.85	96.96	2.41	111
28	17 43 33.13	−29 51 33.11	15.02	10.83	8.42	..	15.00	8.41	4.68	2.88	6.89	6.34	4.78	4.34	4.70	3.60	3.30	98.98	6.38	5.34	4.33	2.92	2.62	96.96	2.96	111
29	17 43 34.79	−29 40 30.41	(16.90)	13.15	9.76	..	..	9.15	4.65	2.96	88.88	88.88	88.88	88.88	4.65	3.42	2.78	98.98	5.37	4.49	3.98	2.30	1.62	96.96	2.90	111
30	17 43 35.12	−29 24 47.22	(18.47)	12.22	9.09	..	..	8.82	4.97	2.95	88.88	88.88	88.88	88.88	4.57	3.13	3.08	98.98	7.61	6.05	4.41	2.63	2.01	..	..	111

Notes. Identification numbers are from Tables 1 and 2 of this work, and from Tables 2 and 3 of Messineo et al. (2002) (see also Table 2 in Messineo et al. (2004)). Magic values are set as follow: .. = general indicator of a missing entry; 98.98 = upper limits; 97.97 = blending ((i) automatically identified by having found multiple WISE stars or multiple GLIMPSE bright stars at this position; (ii) datapoints removed after visual image inspection because of astrometric offsets due to stellar blending or strong nebular emission); 96.96 = area not covered by the survey; 95.95 = faint source not detected; 94.94 = datapoints removed because very offset from the SED defined by the other datapoints; 93.93 = magnitude above the saturation limit; 88.88 = no magnitude was found, but the corresponding image is saturated (bright target). For 2MASS JHK_s bands, upper limits are given between parenthesis.

(†) 2MASS JHK_s magnitudes are missing or blended in 2MASS. UKIDSS coordinates and magnitudes are provided, between parenthesis when affected by saturation.

(∗) These marked Id indicate targets for which multiple WISE sources fall within the beam. There is a small chance that the selected counterparts are not the actual masing stars.

(+) Nstar is a flag that concatenates the number of MSX point sources detected within a radius of 14.″5 (first digit), the number of WISE point sources detected within a radius of 10.″0 (second digit), and the number of preselected GLIMPSE point sources within a radius of 10.″0 (third digit). For example, Nstar=111 means that in the searched circle we found only 1 MSX star, 1 WISE, and 1 bright GLIMPSE. Exception: when the second digit is 9, it means that no WISE target was found in the AllWISE Data Release, and the adopted magnitudes come from the older WISE All-Sky Data Release.

(a) For star #294, there are additional JHK measurements from Cabrera-Lavers et al. (2006) that well agree with the 2MASS (J = 11.333, H = 7.346, K = 5.442 mag). This suggests that the DENIS K_s measurement (7.73 mag) could be affected by artifact.

(∗∗) The full table contains 571 objects and is available in electronic form at the CDS via anonymous ftp to cdsarc.u-strasbg.fr (130.79.128.5) or via http://cdsweb.u-strasbg.fr/cgi-bin/qcat?J/A+A/xxx/xxx.